Exciton-exciton interaction beyond the hydrogenic picture in a MoSe2 monolayer in the strong light-matter coupling regime

Petr Stepanov, Amit Vashisht, Martin Klaas, Nils Lundt, Sefaattin Tongay, Mark Blei, Sven Höfling, Thomas Volz, Anna Minguzzi, Julien Renard, et al.

Exciton-Exciton Interaction beyond the Hydrogenic Picture in a $MoSe_2$ Monolayer in the Strong Light-Matter Coupling Regime

Petr Stepanov,[1] Amit Vashisht,[2] Martin Klaas,[3] Nils Lundt,[3] Sefaattin Tongay,[4] Mark Blei,[4] Sven Höfling,[3] Thomas Volz,[5,6] Anna Minguzzi,[2] Julien Renard,[1] Christian Schneider,[7] and Maxime Richard[1,*]

[1]*Univ. Grenoble Alpes, CNRS, Grenoble INP, Institut Néel, 38000 Grenoble, France*
[2]*Univ. Grenoble Alpes, CNRS, LPMMC, 38000 Grenoble, France*
[3]*Technische Physik and Wilhelm Conrad Röntgen Research Center for Complex Material Systems, Physikalisches Institut, Universität Würzburg, Am Hubland, D-97074 Würzburg, Germany*
[4]*Arizona State University, Tempe, Arizona 85287, USA*
[5]*Department of Physics and Astronomy, Macquarie University, NSW, 2109, Australia*
[6]*ARC Centre of Excellence for Engineered Quantum Systems, Macquarie University, NSW, 2109, Australia*
[7]*Institute of Physics, University of Oldenburg, 26129 Oldenburg, Germany*

(Received 1 July 2020; revised 1 February 2021; accepted 19 March 2021; published 19 April 2021)

In transition metal dichalcogenides' layers of atomic-scale thickness, the electron-hole Coulomb interaction potential is strongly influenced by the sharp discontinuity of the dielectric function across the layer plane. This feature results in peculiar nonhydrogenic excitonic states in which exciton-mediated optical nonlinearities are predicted to be enhanced compared to their hydrogenic counterparts. To demonstrate this enhancement, we perform optical transmission spectroscopy of a $MoSe_2$ monolayer placed in the strong coupling regime with the mode of an optical microcavity and analyze the results quantitatively with a nonlinear input-output theory. We find an enhancement of both the exciton-exciton interaction and of the excitonic fermionic saturation with respect to realistic values expected in the hydrogenic picture. Such results demonstrate that unconventional excitons in $MoSe_2$ are highly favorable for the implementation of large exciton-mediated optical nonlinearities, potentially working up to room temperature.

DOI: 10.1103/PhysRevLett.126.167401

The realization of solid-state photonic nanostructures featuring a large third-order optical nonlinearity is a high stakes objective. Arrays of coupled nonlinear optical microcavities, for instance, would constitute a powerful simulator of nonequilibrium quantum many-body physics [1,2] in which phenomena such as a fractional quantum Hall states [3–5], fermionized states [6], nontrivial topological phenomena [7], and a variety of nonequilibrium quantum phase transitions [8–11] have been predicted. This nonlinearity is also currently a key mechanism in optical communication and computation, as photonic logic gates are mostly built on it [12–16]. Increasing further the nonlinearity lowers the energy required to switch the gate up to a point where the operation works in the quantum regime [17] as required in future quantum computing and communication devices based on photons [18].

In this context, excitonic states, i.e., bound electron-hole pairs in semiconductor nanostructures, are ideally suited. Their dipole moment provides both strong interaction with light and a large third-order optical nonlinearity due (i) to Coulomb interaction between excitons (of magnitude g_x) that shifts the excitonic transition [19] and (ii) to the fermionic saturation (of magnitude g_s) of the involved electrons and holes [20] that reduces the excitonic oscillator strength. In quantum well geometries, which are technologically convenient for fabrication and scalability, a strategy known as polariton quantum blockade [21] maximizes the effective excitonic nonlinearity, in principle up to the quantum regime, by optimizing the coupling with light and optically narrowing down the in-plane excitonic wave function. The onset of this regime has been demonstrated recently in GaAs-based microcavities at cryogenic temperatures [22,23].

For this strategy to deliver its full potential, maximizing both the excitonic nonlinear constants and binding energy (to approach room temperature stability) is crucial. But these quantities are hard to engineer in the conventional semiconductor materials used so far (e.g., arsenide, nitride, telluride, oxides, or cuprate alloys): this class of materials is characterized by a hydrogenic-type excitonic state resulting from a screened but conventional Coulomb potential. In this picture, $g_x \propto \hbar^2/2\mu$ depends only on the exciton reduced mass $\mu^{-1} = m_e^{-1} + m_h^{-1}$, where m_e (m_h) is the electron (hole) effective mass [19] and $g_s \propto \epsilon^2/\mu^2$ [20], where ϵ is the background dielectric constant. Both quantities are thus strongly bound to intrinsic properties of the material and therefore hard to manipulate: arsenide alloys offer a sizeable $g_{x,s}$ but cryogenic temperature stability only and vice versa for, e.g., cuprates or nitride alloys [see Fig. 1(c)].

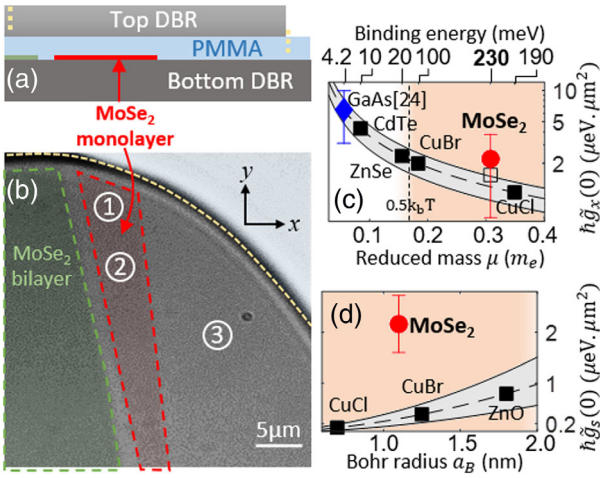

FIG. 1. $MoSe_2$ monolayer microcavity. (a) Outline of the microcavity structure: a $MoSe_2$ monolayer (red) and bilayer (green) embedded in polymethyl methacrylate (PMMA) (pale blue) are sandwiched between two Bragg mirrors (DBR). (b) White light image of the microcavity; the $MoSe_2$ layers have been color shaded and outlined. The experiments performed at 105 K (127 K) were realized in the area labeled (1) [(2)]. The bare cavity measurements have been done in the area labeled (3). (c) $\tilde{g}_x(0)$ dependence on μ, and (d) $\tilde{g}_s(0)$ dependence on a_B. The dashed line and gray area show hydrogenic exciton (HE) theory corrected by a factor $\alpha_0 = 3.3 \pm 0.8$ following [24] (see text). The black squares highlight HE theory for CdTe, ZnSe, ZnO, CuBr, and CuCl [25]. The hollow square shows the 30% enhanced HE theory for $MoSe_2$ [54]. The blue diamond is a measurement in a GaAs microcavity taken from [24]. Our best measurements are shown as red circles. The upper axis in (c) indicates the bulk exciton binding energy for each material [25]. Room-temperature-stable excitons are on the right side of the vertical dashed line [25].

Monolayers of semiconductor transition metal dichalcogenides (TMDCs) [55] offer a unique opportunity to manipulate the excitonic nonlinearity beyond this trade-off. Owing to their atomic-scale thickness, the dielectric constant exhibits a sharp discontinuity across the material plane that results in a strongly modified Coulomb potential [56] and a high sensitivity to the dielectric environment surrounding the layer. The resulting excitonic states are uniquely nonhydrogenic [57,58] and highly tunable via van der Waals heterostructure engineering [59], and their nonlinear constants g_x and g_s are expected to deviate from the hydrogenic picture. A 30% enhancement of g_x is, for instance, predicted in WS_2 [54]. Some indications of sizeable excitonic nonlinearities have been observed in TMDCs [60], in charged [61] and excited states of excitons [62], and in polaron-polaritons [63].

In this work, we take advantage of the giant oscillator strength of TMDCs excitons [64–67] to put a $MoSe_2$ monolayer in the strong coupling regime with the resonance of a microcavity [68–70] and carry out spatially resolved optical transmission spectroscopy with pulsed laser light as a function of the intensity. The obtained spectra exhibit signatures of a nonlinear response from which we derive a quantitative estimate of g_s, g_x, and the polarization dependence of the latter. The monolithic microcavity that we investigate is shown in Figs. 1(a) and 1(b) with its main features highlighted (see [25,70] for details). The microcavity's quality factor and Rabi splitting amount to $Q \simeq 730$ and $\hbar\Omega = 28 \pm 3$ meV, respectively. The latter is derived from the anticrossing of the polariton modes that we observe in a transmission measurement upon sweeping temperature. Details of this characterization can be found in [25].

We then move on to the nonlinear transmission measurements. We use a pulsed Ti:sapphire laser that delivers ~200 fs pulses with a spectrum $I_{\rm las}(\omega)$ of tunable mean energy $\hbar\omega_{\rm las} = [1640, 1660]$ meV and a bandwidth $\gamma_{\rm las} \sim 10$ meV. Its purpose is the ultrafast creation of a dense polariton population resonantly, without overheating the sample, and to perform a broadband transmission spectrum measurement that is able to capture both the lower and upper polaritons. Heating from residual absorption is further suppressed by chopping the laser into a 0.7% on-off duty cycle. The beam is prepared into a Gaussian mode that is focused on the microcavity surface into a $\sigma = 5.8$ μm waist size spot. We use a quarter-wave plate to tune the laser polarization among the states $|\theta\rangle$, where $|\theta\rangle = \sin(2\theta)/\sqrt{2}|x\rangle + [i + \cos(2\theta)]/\sqrt{2}|y\rangle$, $|x, y\rangle$ is the linear polarization basis oriented as shown in Fig. 1(b), and θ is the wave plate rotation angle with respect to y. In the first part of this work, we use y-polarized light ($\theta = 0$). The time-integrated transmitted light intensity I_T is collected with a microscope objective and imaged at the entrance focal plane of a 300 grooves/mm grating spectrometer. By doing so, we obtain space and frequency-resolved transmission spectra $T(\omega, y) = I_T(\omega, y)/I_{\rm las}(\omega, y)$. Since our aim is to provide a quantitative estimate of the interactions, we also need to know the electromagnetic energy W in each pulse. To do so, the time-averaged laser power $P_{\rm las}$ is measured at the input cryostat window just before the laser light impinges the cavity backside using a thermal-head power meter. $T(\omega, y)$ is thus measured from $W_0 = 0.1$ pJ, which is well below the onset of the nonlinear regime, up to several hundreds of pJ, which is well above.

Two such measurements, realized in areas (1) and (2), at temperatures $T = 127$ K and $T = 105$ K, respectively, are shown in Figs. 2(a) and 2(b). The excitonic fraction of the polariton field in each case is $|X|^2 = 0.48$ and $|X|^2 = 0.33$, respectively. We indeed exploit the fact that the excitonic transition energy is temperature-dependent to control the detuning $\Delta(T) = \omega_{c,0} - \omega_x(T)$ between the bare cavity (frequency $\omega_{c,0}$) and the excitonic level (frequency ω_x) [25] and hence the excitonic fraction $|X|^2$ ($|C|^2 = 1 - |X|^2$) of the lower (upper) polariton states [71]. The effective polariton-polariton interaction constant is thus varied as it

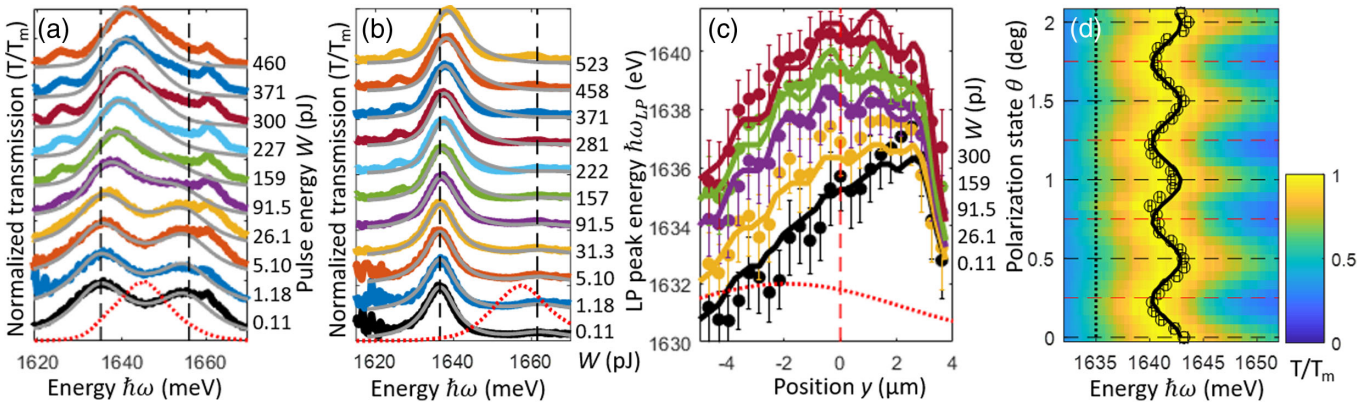

FIG. 2. Nonlinear transmission spectroscopy. Measured normalized transmission spectra $T(\omega)/\mathrm{Max}(T)$ at $T = 127$ K (a) and $T = 105$ K (b). The spectra are stacked from the lowest used pulse energy W (bottom) to the highest (top). The pulse energy W used for each spectrum is indicated on the right axis. The laser pulse spectrum is shown in (a),(b) as a red dotted line. The dashed vertical black lines in (a),(b) highlight the polaritonic resonances in the linear regime. The theoretical fits are shown as solid gray lines. (c) Spatially resolved lower polariton transmission peak energy measured at $T = 127$ K, across the excitation spot diameter, for increasing W [same color code as in (a)]. The spatial laser intensity profile is shown as a red dotted line. The spectra in (a) have been measured at $y = 0$ (dashed vertical line). (d) Color-scaled normalized transmission spectra at $W = 451$ pJ versus the polarization state $|\theta\rangle$ (vertical axis). The circle symbols show the lower polariton peak energy; the solid black line is a theoretical fit $B_0 + B_\theta \sin^2 2\theta$ following Eqs. (3) and (4), where $B_0 = 7.9$ meV and $B_\theta = -2.7$ meV.

depends on $|X|^2$ [20,25]. The laser pulse spectral overlap with the polariton modes is also different in the two experiments. We take advantage of these variations to test the robustness of our quantitative estimate of g_s and g_x, as they should not depend on these parameters. The plotted transmission spectra are normalized to their maximum T_m for clearer representation. In the linear regime (bottom spectra, $W = 0.11$ pJ), we observe both the upper and lower polariton resonances with a mostly equal weight at $T = 127$ K and with a dominant lower polariton peak at $T = 105$ K, which is consistent with their respective photonic fractions. Two smaller peaks are also visible in these spectra, at $\hbar\omega = 1625.6$ meV and $\hbar\omega = 1660.4$ meV, that we traced back, by real space analysis, to bare cavity resonances situated within the small gap separating the $MoSe_2$ monolayer from the bilayer. Upon increasing W, the polaritonic resonances exhibit a clear and consistent trend: at moderate W, the lower polariton peak blueshifts, while the upper polariton essentially does not. This behavior difference is key to distinguish between the contributions of g_s and g_x to the nonlinearity. Indeed, while the Coulomb interaction contributes to the blueshifting of both lower and upper polaritons, the saturation causes a reduction of the effective Rabi spitting and thus shifts the lower and upper polaritons in opposite directions [25]. The trend we observe thus indicates that the saturation contributes significantly to the nonlinearity, which is consistent with recent reports [72].

We interpret these spectra quantitatively by theoretical simulation of the polariton field ultrafast evolution, including the shape of the laser pulse in time and space. Specifically, we derive a mean-field input-output theory in the exciton-photon basis [25] that includes exciton-exciton interaction and saturation at first order in the interaction strength. Note that exciton-exciton-induced broadening is a second-order contribution [73], which is typically ten times smaller than the first-order ones in TMDCs [66]. Owing to the exciton spin properties, g_x has two contributions, $g_{x,\parallel}$ and $g_{x,\perp}$, corresponding to the interactions between parallel and opposite spin excitons, that couple to co- and cross-circularly polarized light. After transformation into the θ polarization basis, the equation of motion for the exciton and photon fields $\psi_{x,c}(\boldsymbol{r}, t)$ read

$$i\partial_t\psi_c = \left[\omega_{c,0} - \frac{\hbar}{2m}\nabla^2 - i\frac{\gamma_c}{2} + V_c(\boldsymbol{r})\right]\psi_c + \left[\frac{\Omega}{2} - \frac{\tilde{g}_s(\theta)}{2}|\psi_x|^2\right]\psi_x + \sqrt{2\gamma_{\mathrm{in}}}A_{\mathrm{in}} \quad (1)$$

$$i\partial_t\psi_x = \left[\omega_{x,0} - i\frac{\gamma_x}{2} + V_x(\boldsymbol{r}) + \tilde{g}_x(\theta)|\psi_x|^2\right]\psi_x + \left(\frac{\Omega}{2} - \tilde{g}_s(\theta)|\psi_x|^2\right)\psi_c - \frac{\tilde{g}_s(\theta)}{2}\psi_x^2\psi_c^*, \quad (2)$$

where $A_{\mathrm{in}}(\boldsymbol{r}, t)$ is the θ-polarized incident laser pulse field density, $\omega_{c,0}/2\pi$ is the bare cavity resonance frequency at vanishing in-plane wave vector $k_\parallel = 0$, m its effective mass, $\omega_{x,0}/2\pi$ is the excitonic transition frequency, of which we can neglect the kinetic contribution, and $\hbar\Omega$ is the Rabi splitting. γ_x is the excitonic nonradiative relaxation rate, $\gamma_c = \gamma_{\mathrm{in}} + \gamma_{\mathrm{out}}$ is the cavity radiative decay rate, and γ_{in} (γ_{out}) are the cavity coupling rate on the laser input side (of the transmission side). $V_c(\boldsymbol{r})$ and $V_x(\boldsymbol{r})$ describe the

spatial fluctuations of the cavity resonance and of the excitonic transition. Finally, $\tilde{g}_s(\theta)$, and $\tilde{g}_x(\theta)$ are the saturation and exciton-exciton interaction constants in the θ-polarization basis given by [25]

$$\tilde{g}_x(\theta) = \frac{1}{2}(g_{x,\parallel} + g_{x,\perp}) + \frac{1}{2}(g_{x,\parallel} - g_{x,\perp})\sin^2(2\theta), \quad (3)$$

$$\tilde{g}_s(\theta) = \frac{g_s}{2}[1 + \sin^2(2\theta)]. \quad (4)$$

Note that in Eqs. (1) and (2) we have neglected the contribution of the cross-polarized $\bar{\theta}$ components of the exciton and photon fields since the laser excites only one θ component and the interactions terms provide only density-mediated couplings that vanish if one of the two fields is zero. We also checked experimentally that the polariton modes exhibit no birefringence [25].

In order to fully account for the time profile of the excitation pulse and the Gaussian shape of the spot in real space, we solved this model numerically. The experimental parameters entering the model are the microcavity and laser characteristics, which are known accurately. The interaction constants $\tilde{g}_x(\theta)$ and $\tilde{g}_s(\theta)$ are thus the only free parameters. We first apply this model to the spectra shown in Figs. 2(a) and 2(b) (in the $\theta = 0$ polarization state). $\tilde{g}_x(0) = (g_{x,\parallel} + g_{x,\perp})/2$ and $\tilde{g}_s(0) = g_s/2$ are thus derived with their uncertainty by numerical optimization of the fit between the model and the measurements [25]. This analysis yields $\tilde{g}_x(0) = 2.2 \pm 1.6\mu$ eV. μm^2 and $\tilde{g}_s(0) = 2.16 \pm 0.5\ \mu\text{eV} \cdot \mu\text{m}^2$ for the experiment at $T = 127$ K shown in Fig. 2(a). The experiment at $T = 105$ K consistently yields $\tilde{g}_x(0) = 4.3\ \mu\text{eV} \cdot \mu\text{m}^2$ and $\tilde{g}_s(0) = 1.6\ \mu\text{eV} \cdot \mu\text{m}^2$, albeit with a much larger uncertainty due to the fact that the upper polariton contribution to the spectra is small and hence prevents determining accurately the relative contribution of $\tilde{g}_x(0)$ and $\tilde{g}_s(0)$. We also derive the excitonic densities (HWHM in time and space) that increases from $5 \times 10^8\text{cm}^{-2}$ ($W = 0.11$ pJ) to $9 \times 10^{11}\text{cm}^{-2}$ ($W = 460$ pJ). Note that at high W, the saturation effect is large and our model is expected to overestimate it in this regime [20,61,74,75]. This is indeed the trend that we observe in the last four spectra in Fig. 2(b), in which the theory predicts a slightly smaller Rabi splitting than in the experiment. Yet, except for this feature, the spectral shape and peak energies evolution for increasing W are in very good agreement with the experiment.

We cross-checked this quantitative analysis by looking at another footprint of the nonlinearity: the nontrivial spatially dependent transmission spectrum $T(y,\omega)/T_m$ that results from the interplay between the Gaussian shape of the spot and the nonlinearity. Figure 2(c) shows the lower polariton transmission peak energy $E_{\text{lp}}(y)$ plotted versus y, where y is the position along a diameter of the laser spot and $y = 0$ is the laser spot intensity maximum position. The lowest spectrum (black) is obtained in the linear regime ($W = 0.11$ pJ) and thus shows the lower polariton potential $V(y)$, from which we derive $V_c(y)$. For increasing W, the nonlinearity changes this shape as the blueshift depends on the local density and excitonic fraction. We can fit this behavior quantitatively with our model, and a good agreement is obtained for $\tilde{g}_x(0) = 4.3^{+30}_{-4}\ \mu\text{eV} \cdot \mu\text{m}^2$ and $\tilde{g}_s(0) = 3.2 \pm 0.8\ \mu\text{eV} \cdot \mu\text{m}^2$. The large uncertainty reflects the fact that the upper polariton contribution is weak in the dataset, and the relative contributions of $g_x(0)$ and $g_s(0)$ are hard to distinguish. Yet, the result is consistent with the spectral analysis.

We verified that the nonlinearities that we measure in this Letter come from the monolayer and not from any other materials within the structure. We thus measured $T(\omega)/T_m$ in area (3), which is a bare cavity free from $MoSe_2$. The area exhibits a sharp cavity mode that does not shift [$\hbar\delta\omega_c(W) = 0 \pm 0.025$ meV] up to the highest applied pulse energy ($W = 1.12$ nJ), as shown in detail in [25]. We also examined the possible co-excitation of a dark exciton reservoir alongside polaritons, as is often the case in arsenide microcavities [76–79]. We looked for its signature in a time-resolved transmission measurement and found none, meaning that the reservoir, if any, has a poor quantum yield. Using realistic parameters and conservative assumptions, we could determine that such a reservoir would typically decrease $\tilde{g}_{x,s}(0)$ by ~35% [25].

In Figs. 1(c) and 1(d), we plotted the theoretical HE interaction constants $\tilde{g}_x(0) \simeq 3\alpha_0\hbar^2/2\mu$ (in which we assumed that $|g_\perp| \ll g_\parallel$) versus μ and $\tilde{g}_s(0) = \alpha_0^2(2\pi/7)\hbar\Omega a_B^2$ versus a_B (dashed lines). $\alpha_0 = 3.3 \pm 0.8$ is introduced in order for the theory to agree quantitatively with the measurement in Estrecho *et al.* [24], where $g_{x,\parallel} = 13 \pm 3.4\ \mu\text{eV} \cdot \mu\text{m}^2$ is found for a planar microcavity with GaAs quantum wells [25]. This deviation might arise from the strict 2D approximation of the excitonic wave function in the theory, which is likely inaccurate in realistic quantum wells [24]. Using excitonic reduced masses from the literature [25], a few materials are highlighted (squares) along these theoretical curves. In Fig. 1(c), the bulk exciton binding energies are also indicated for each material on the top axis as reference [25]. The measurements obtained from the analysis of Fig. 2(a) are shown as a red circle in Figs. 1(c) and 1(d). Our measured $\tilde{g}_x(0)$ is found to moderately exceed hydrogenic exciton (HE's) theory and is fully compatible with the 30% enhancement [hollow square in Fig. 1(c)] predicted in [54], while $\tilde{g}_s(0)$ exceeds HE's theory by a large factor: 7 ± 2. A possible origin of this larger deviation is already visible in the HE picture, in which g_s depends directly on the dielectric function square (via a_B), while g_x essentially does not.

Finally, we characterized the spin anisotropy of the nonlinearity at $T = 127$ K during the same experimental run as that shown in Fig. 2(a) by measuring the transmission spectrum versus θ. The results are shown in

Fig. 2(d): upon increasing θ from 0 (linear polarization) to $\pi/4$ (circular polarization) at a fixed $W = 451$ pJ, the spectrum exhibits a global redshift of 2.7 meV. Using our model and Eqs. (3) and (4) [25], this behavior implies that $g_{x,\perp}$ is about two times larger than $g_{x,\parallel}$ and positive. In TMDC monolayers [54], like in conventional materials, the Coulomb interaction between polaritons is in principle dominated by exchange interaction [19] for which $g_{x,\perp}$ is expected to be negative and small compared to $g_{x,\parallel}$ [80,81]. Our result differs from this picture and is thus highly nontrivial. Its precise interpretation requires a fully dedicated investigation that exceeds the scope of the present work.

A possible explanation could be the involvement of an intermediate state such as spin-2 dark excitons [80] or biexcitons [82,83]. In such a mechanism, $g_{x,\perp}$ is enhanced and takes a positive sign when the two-polariton state is close and on the high energy side of the intermediate state. In a $MoSe_2$ monolayer, the dark exciton state is a few meV above the bright one [84], such that the upper polariton state, nominally 12.2 meV above the bright exciton, could benefit from this resonance at the peak intensity when the saturation brings it closer. A resonance with the biexciton state is expected 10 meV [85,86] below the bright exciton, which is 3 meV above the nominal energy of the lower polariton and thus also favorable at the peak intensity. Finally, at such a large W, higher order many-body correlations and the composite nature of excitons might start to contribute such that our estimate of $g_{x,\perp}$ might be too inaccurate. Yet, owing to the robustness that the model has demonstrated in reasonably capturing the measurements in Figs. 2(a)–2(c), we expect that this estimate is at least qualitatively correct—namely, that $g_{x,\perp}$ is positive and comparable in magnitude to $g_{x,\parallel}$ and g_s.

In summary, we have shown that owing to the nonhydrogenic character of excitons, a $MoSe_2$ monolayer in the strong coupling regime displays enhanced exciton-mediated optical nonlinearity, in particular via the excitonic saturation mechanism. We also observe a nontrivial spin anisotropy of the interaction that deserves future investigation. Our results demonstrate that nonhydrogenic exciton in $MoSe_2$ and in other TMDC materials, where the nonlinearity enhancement could be potentially even larger, offer new perspectives for the engineering of exciton-mediated optical nonlinearities.

The authors acknowledge fruitful discussions with D. Basko, O. Kyriienko, and D. Ferrand. P. S., M. R., and J. R. are supported by the French National Research Agency in the framework of the Investissements d'Avenir program (ANR-15-IDEX-02) and by the research Grant No. ANR-16-CE30-0021. S. T. acknowledges support from NSF DMR 1838443 and ARO Materials STIR program. M. K., N. L., S. H., and C. S. acknowledge support by the State of Bavaria. C. S. acknowledges support by the European Research Commission (ERC, Project unLiMIt-2D, 697228). T. V. acknowledges the ARC Centre of Excellence for Engineered Quantum Systems (CE170100009). A. V. acknowledges the European Union Horizon 2020 research and innovation program under the Marie Skłodowska-Curie Grant Agreement No. 754303.

P. S. and A. V. contributed equally to this work.

*Corresponding author.
maxime.richard@neel.cnrs.fr

[1] A. Tomadin and R. Fazio, J. Opt. Soc. Am. B **27**, A130 (2010).
[2] C. Noh and D. G. Angelakis, Rep. Prog. Phys. **80**, 016401 (2017).
[3] J. Cho, D. G. Angelakis, and S. Bose, Phys. Rev. Lett. **101**, 246809 (2008).
[4] R. O. Umucalilar and I. Carusotto, Phys. Rev. Lett. **108**, 206809 (2012).
[5] M. Hafezi, M. D. Lukin, and J. M. Taylor, New J. Phys. **15**, 063001 (2013).
[6] I. Carusotto, D. Gerace, H. E. Tureci, S. De Liberato, C. Ciuti, and A. Imamoglu, Phys. Rev. Lett. **103**, 033601 (2009).
[7] J. Tangpanitanon, V. M. Bastidas, S. Al-Assam, P. Roushan, D. Jaksch, and D. G. Angelakis, Phys. Rev. Lett. **117**, 213603 (2016).
[8] A. Tomadin, V. Giovannetti, R. Fazio, D. Gerace, I. Carusotto, H. E. Türeci, and A. Imamoglu, Phys. Rev. A **81**, 061801(R) (2010).
[9] J. Jin, D. Rossini, R. Fazio, M. Leib, and M. J. Hartmann, Phys. Rev. Lett. **110**, 163605 (2013).
[10] J. Jin, D. Rossini, M. Leib, M. J. Hartmann, and R. Fazio, Phys. Rev. A **90**, 023827 (2014).
[11] J. Raftery, D. Sadri, S. Schmidt, H. E. Türeci, and A. A. Houck, Phys. Rev. X **4**, 031043 (2014).
[12] P. Andalib and N. Granpayeh, J. Opt. Soc. Am. B **26**, 10 (2009).
[13] Y. Liu, F. Qin, Z.-M. Meng, F. Zhou, Q.-H. Mao, and Z.-Y. Li, Opt. Express **19**, 1945 (2011).
[14] H. Mabuchi, Appl. Phys. Lett. **99**, 153103 (2011).
[15] T. Espinosa-Ortega and T. C. H. Liew, Phys. Rev. B **87**, 195305 (2013).
[16] A. Salmanpour, S. Mohammadnejad, and A. Bahrami, Opt. Quantum Electron. **47**, 2249 (2015).
[17] F. Flamini, N. Spagnolo, and F. Sciarrino, Rep. Prog. Phys. **82**, 016001 (2019).
[18] J. L. OBrien, A. Furusawa, and J. Vuckovic, Nat. Photonics **3**, 687 (2009).
[19] C. Ciuti, V. Savona, C. Piermarocchi, A. Quattropani, and P. Schwendimann, Phys. Rev. B **58**, 7926 (1998).
[20] G. Rochat, C. Ciuti, V. Savona, C. Piermarocchi, A. Quattropani, and P. Schwendimann, Phys. Rev. B **61**, 13856 (2000).
[21] A. Verger, C. Ciuti, and I. Carusotto, Phys. Rev. B **73**, 193306 (2006).
[22] G. Munoz Matutano *et al.*, Nat. Mater. **18**, 213 (2019).

[23] A. Delteil, T. Fink, A. Schade, S. Höfling, C. Schneider, and A. İmamoğlu, Nat. Mater. **18**, 219 (2019).
[24] E. Estrecho *et al.*, Phys. Rev. B **100**, 035306 (2019).
[25] See Supplemental Material, which includes Refs. [20,26–53], at http://link.aps.org/supplemental/10.1103/PhysRevLett.126.167401 for details on the experiment, the theory, and the data analysis.
[26] A. Castellanos-Gomez, M. Buscema, R. Molenaar, V. Singh, L. Janssen, H. S. J. van der Zant, and G. A. Steele, 2D Mater. **1**, 011002 (2014).
[27] A. Arora, K. Nogajewski, M. Molas, M. Koperski, and M. Potemski, Nanoscale **7**, 20769 (2015).
[28] D. V. Vishnevsky, D. D. Solnyshkov, N. A. Gippius, and G. Malpuech, Phys. Rev. B **85**, 155328 (2012).
[29] T. K. Paraïso, M. Wouters, Y. Leger, F. Morier-Genoud, and B. Deveaud-Pledran, Nat. Mater. **9**, 655 (2010).
[30] C. Robert *et al.*, Phys. Rev. B **93**, 205423 (2016).
[31] N. B. Mohamed, F. Wang, H. E. Lim, W. Zhang, S. Koirala, S. Mouri, Y. Miyauchi, and K. Matsuda, Phys. Status Solidi B **254**, 1600563 (2017).
[32] N. B. Mohamed, H. E. Lim, F. Wang, S. Koirala, S. Mouri, K. Shinokita, Y. Miyauchi, and K. Matsuda, Appl. Phys. Express **11**, 015201 (2018).
[33] W. Nakwaski, Physica (Amsterdam) **210B**, 1 (1995).
[34] P. E. Simmonds, M. J. Birkett, M. S. Skolnick, W. I. E. Tagg, P. Sobkowicz, G. W. Smith, and D. M. Whittaker, Phys. Rev. B **50**, 11251(R) (1994).
[35] J. Christen, D. Bimberg, A. Steckenborn, and G. Weimann, Appl. Phys. Lett. **44**, 84 (1984).
[36] L. S. Dang, G. Neu, and R. Romestain, Solid State Commun. **44**, 1187 (1982).
[37] R. André *et al.*, J. Cryst. Growth **184–185**, 758 (1998).
[38] J. Duan, L. Song, and J. Zhan, Nano Res. **2**, 61 (2009).
[39] C. S. Wang and B. M. Klein, Phys. Rev. B **24**, 3393 (1981).
[40] S. Adachi and T. Taguchi, Phys. Rev. B **43**, 9569 (1991).
[41] T. Miyajima, F. P. Logue, J. F. Donegan, J. Hegarty, H. Okuyama, A. Ishibashi, and Y. Mori, Appl. Phys. Lett. **66**, 180 (1995).
[42] S. Hong, T. Joo, W. I. Park, Y. H. Jun, and G.-C. Yi, Appl. Phys. Lett. **83**, 4157 (2003).
[43] K. K. Nanda, F. E. Kruis, H. Fissan, and S. N. Behera, J. Appl. Phys. **95**, 5035 (2004).
[44] U. Woggon, O. Wind, W. Langbein, O. Gogolin, C. Klingshirn, J. Photolum. **59**, 135 (1994).
[45] U. Woggon, O. Wind, W. Langbein, O. Gogolin, and C. Klingshirn, J. Lumin. **59**, 135 (1994).
[46] T. Mita, K. Sotome, and M. Ueta, Solid State Commun. **33**, 1135 (1980).
[47] Z. K. Tang, A. Yanase, T. Yasui, Y. Segawa, and K. Cho, Phys. Rev. Lett. **71**, 1431 (1993).
[48] Z. K. Tang, A. Yanase, Y. Segawa, N. Matsuura, and K. Cho, Phys. Rev. B **52**, 2640 (1995).
[49] A. Kormanyos *et al.*, 2015 2D Mater. **2**, 022001 (2015).
[50] M. M. Ugeda *et al.*, Nat. Mater. **13**, 1091 (2014).
[51] M. Goryca, J. Li, A. V. Stier, T. Taniguchi, K. Watanabe, E. Courtade, S. Shree, C. Robert, B. Urbaszek, X. Marie, and S. A. Crooker, Nat. Commun. **10**, 4172 (2019).
[52] H. Mathieu, P. Lefebvre, and P. Christol, Phys. Rev. B **46**, 4092 (1992).
[53] C. Ciuti and I. Carusotto, Phys. Rev. A **74**, 033811 (2006).
[54] V. Shahnazaryan, I. Iorsh, I. A. Shelykh, and O. Kyriienko, Phys. Rev. B **96**, 115409 (2017).
[55] G. Wang, A. Chernikov, M. M. Glazov, T. F. Heinz, X. Marie, T. Amand, and B. Urbaszek, Rev. Mod. Phys. **90**, 021001 (2018).
[56] L. V. Keldysh, JETP Lett. **29**, 658 (1979), https://ui.adsabs.harvard.edu/#abs/1979JETPL..29..658K/abstract.
[57] T. C. Berkelbach, M. S. Hybertsen, and D. R. Reichman, Phys. Rev. B **88**, 045318 (2013).
[58] A. Chernikov, T. C. Berkelbach, H. M. Hill, A. Rigosi, Y. Li, O. B. Aslan, D. R. Reichman, M. S. Hybertsen, and T. F. Heinz, Phys. Rev. Lett. **113**, 076802 (2014).
[59] Y. Liu, N. O. Weiss, X. Duan, H.-C. Cheng, Y. Huang, and X. Duan, Nat. Rev. Mater. **1**, 16042 (2016).
[60] F. Barachati, A. Fieramosca, S. Hafezian, J. Gu, B. Chakraborty, D. Ballarini, L. Martinu, V. Menon, D. Sanvitto, and S. Kéna-Cohen, Nat. Nanotechnol. **13**, 906 (2018).
[61] R. P. A. Emmanuele *et al.*, Nat. Commun. **11**, 3589 (2020).
[62] G. Scuri *et al.*, Phys. Rev. Lett. **120**, 037402 (2018).
[63] L. B. Tan, O. Cotlet, A. Bergschneider, R. Schmidt, P. Back, Y. Shimazaki, M. Kroner, and A. Imamoglu, Phys. Rev. X **10**, 021011 (2020).
[64] C. Poellmann, P. Steinleitner, U. Leierseder, P. Nagler, G. Plechinger, M. Porer, R. Bratschitsch, C. Schüller, T. Korn, and R. Huber, Nat. Mater. **14**, 889 (2015).
[65] C. Robert *et al.*, Phys. Rev. B **93**, 205423 (2016).
[66] G. Moody *et al.*, Nat. Commun. **6**, 8315 (2015).
[67] T. Korn, S. Heydrich, M. Hirmer, J. Schmutzler, and C. Schüller, Appl. Phys. Lett. **99**, 102109 (2011).
[68] S. Dufferwiel *et al.*, Nat. Commun. **6**, 8579 (2015).
[69] M. Sidler, P. Back, O. Cotlet, A. Srivastava, T. Fink, M. Kroner, E. Demler, and A. Imamoglu, Nat. Phys. **13**, 255 (2017).
[70] N. Lundt *et al.*, Nat. Nanotechnol. **14**, 770 (2019).
[71] I. Carusotto and C. Ciuti, Rev. Mod. Phys. **85**, 299 (2013).
[72] J. Gu *et al.*, arXiv:1912.12544.
[73] F. Boldt, K. Henneberger, and V. May, Phys. Status Solidi B **130**, 675 (1985).
[74] M. Combescot, O. Betbeder-Matibeta, and F. Dubin, Phys. Rep. **463**, 215 (2008).
[75] O. Kyriienko, D. N. Krizhanovskii, and I. A. Shelykh, Phys. Rev. Lett. **125**, 197402 (2020).
[76] A. V. Sekretenko, S. S. Gravrilov, and V. D. Kulakovskii, Phys. Rev. B **88**, 195302 (2013).
[77] M. Wouters, T. K. Paraïso, Y. Léger, R. Cerna, F. Morier-Genoud, M. T. Portella-Oberli, and B. Deveaud-Plédran, Phys. Rev. B **87**, 045303 (2013).
[78] P. M. Walker, L. Tinkler, B. Royall, D. V. Skryabin, I. Farrer, D. A. Ritchie, M. S. Skolnick, and D. N. Krizhanovskii, Phys. Rev. Lett. **119**, 097403 (2017).
[79] P. Stepanov, I. Amelio, J.-G. Rousset, J. Bloch, A. Lemaitre, A. Amo, A. Minguzzi, I. Carusotto, and M. Richard, Nat. Commun. **10**, 3869 (2019).
[80] M. M. Glazov, H. Ouerdane, L. Pilozzi, G. Malpuech, A. V. Kavokin, and A. D'Andrea, Phys. Rev. B **80**, 155306 (2009).
[81] M. S. Vladimirova, S. Cronenberger, D. Scalbert, K. V. Kavokin, A. Miard, A. Lemaître, J. Bloch, D. Solnyshkov,

G. Malpuech, and A. V. Kavokin, Phys. Rev. B **82**, 075301 (2010).
[82] N. Takemura, M. D. Anderson, M. Navadeh-Toupchi, D. Y. Oberli, M. T. Portella-Oberli, and B. Deveaud, Phys. Rev. B **95**, 205303 (2017).
[83] I. Carusotto, T. Volz, and A. Imamoglu, Europhys. Lett. **90**, 37001 (2010).
[84] C. Robert *et al.*, Nat. Commun. **11**, 4037 (2020).
[85] K. Hao, J. F. Specht, P. Nagler, L. Xu, K. Tran, A. Singh, C. K. Dass, C. Schüller, T. Korn, M. Richter, A. Knorr, X. Li, and G. Moody, Nat. Commun. **8**, 15552 (2017).
[86] O. Bleu, G. Li, J. Levinsen, and M. Parish, Phys. Rev. Research **2**, 043185 (2020).